◆ Human Brain Mapping 32:382–396 (2011) ◆

CENTS: Cortical Enhanced Neonatal Tissue Segmentation

Feng Shi,[1] Dinggang Shen,[1]* Pew-Thian Yap,[1] Yong Fan,[1] Jie-Zhi Cheng,[1] Hongyu An,[2] Lawrence L. Wald,[3,4] Guido Gerig,[5] John H. Gilmore,[6] and Weili Lin[2]

[1]*IDEA Lab, Department of Radiology and BRIC, University of North Carolina at Chapel Hill, Chapel Hill, North Carolina*
[2]*MRI Lab, Department of Radiology and BRIC, University of North Carolina at Chapel Hill, Chapel Hill, North Carolina*
[3]*Department of Radiology, Massachusetts General Hospital, A.A. Martinos Center for Biomedical Imaging, Charlestown, Massachusetts*
[4]*Harvard-MIT Division of Health Sciences and Technology, Cambridge, Massachusetts*
[5]*Scientific Computing and Imaging Institute, University of Utah, Salt Lake City, Utah*
[6]*Department of Psychiatry, University of North Carolina at Chapel Hill, Chapel Hill, North Carolina*

Abstract: The acquisition of high-quality magnetic resonance (MR) images of neonatal brains is largely hampered by their characteristically small head size and insufficient tissue contrast. As a result, subsequent image processing and analysis, especially brain tissue segmentation, are often affected. To overcome this problem, a dedicated phased array neonatal head coil is utilized to improve MR image quality by augmenting signal-to-noise ratio and spatial resolution without lengthening data acquisition time. In addition, a specialized hybrid atlas-based tissue segmentation algorithm is developed for the delineation of fine structures in the acquired neonatal brain MR images. The proposed tissue segmentation method first enhances the sheet-like cortical gray matter (GM) structures in the to-be-segmented neonatal image with a Hessian filter for generation of a cortical GM confidence map. A neonatal population atlas is then generated by averaging the presegmented images of a population, weighted by their cortical GM similarity with respect to the to-be-segmented image. Finally, the neonatal population atlas is combined with the GM confidence map, and the resulting enhanced tissue probability maps for each tissue form a hybrid atlas is used for atlas-based segmentation. Various experiments are conducted to compare the segmentations of the proposed method with manual segmentation (on both images acquired with a dedicated phased array coil and a conventional volume coil), as well as with the segmentations of two population-atlas-based methods. Results show the proposed method is capable of segmenting the neonatal brain with the best accuracy, and also preserving the most structural details in the cortical regions. *Hum Brain Mapp 32:382–396, 2011.*

Key words: neonatal segmentation; tissue segmentation; subject-specific atlas; atlas construction

Contract grant sponsor: NIH; Contract grant number: EB006733, EB008760, EB008374, EB009634, NS055754, MH064065, MH088520, MH070890, HD053000.

*Correspondence to: Dinggang Shen, Department of Radiology and BRIC, University of North Carolina at Chapel Hill, MRI Building, 106 Mason Farm Road, Chapel Hill, NC 27599-7515. E-mail: dgshen@med.unc.edu

Received for publication 11 August 2009; Revised 17 November 2009; Accepted 18 January 2010

DOI: 10.1002/hbm.21023

Published online 5 August 2010 in Wiley Online Library (wileyonlinelibrary.com).

INTRODUCTION

Tissue segmentation, which partitions brain magnetic resonance (MR) images into gray matter (GM), white matter (WM), and cerebrospinal fluid (CSF), is a crucial step for subsequent volumetric and cortical surface analysis. However, effective segmentation of neonatal brain images still remains a great challenge in many emerging neonatal studies, which have the potential of revealing interesting brain developmental patterns and also neurodevelopmental disorders. In particular, two major factors confound neonatal tissue segmentation: (1) the inability of current imaging techniques to acquire neonatal brain images with sufficiently high resolution and signal-to-noise ratio (SNR) for tissue segmentation, and (2) the lack of prior knowledge for a more informed and guided segmentation. In this article, we address both of these issues. First, a dedicated neonatal phased array coil is devised to improve the SNR as well as spatial resolution. Second, a hybrid atlas, combining both the enhanced subject-specific cortical structural characteristics and also population probability maps, is constructed to improve the accuracy of neonatal brain tissue segmentation.

Normally, the brain volume of a neonate is about one half of an adult [Knickmeyer et al., 2008]. As a result, spatial resolution of neonatal brain images is substantially limited, particularly when data acquisition time is a constraint. Moreover, rapid dynamic WM changes due to the ongoing myelination process in the neonatal brain [Connors et al., 2008] further complicates the differentiation between GM and WM. In particular, GM and WM tissue contrast in neonates is manifested in an inverted fashion when compared with that of adults. All these factors confound the acquisition of good quality neonatal brain MR images, the effectiveness of brain tissue segmentation, and hence the accuracy of subsequent image analysis. To improve MR image quality without lengthening data acquisition time, a dedicated phased array neonatal head coil is devised. In a conventional MR imaging session, a volume coil (independent of age) covering the whole brain is utilized. However, it is a known fact that a surface coil with a smaller diameter and thus a smaller sensitivity region can achieve higher SNR in comparison with a volume coil [Roemer et al., 1990]. It is hence possible that multiple smaller coils can be arranged in such a way that a larger region of interest (ROI) can be covered. In doing so, the resulting phased array coil capitalizes the advantages of surface coils in improving SNR and at the same time covers a larger ROI. In addition, coupled with parallel imaging technologies, it yields images with improved quality compared with images acquired using conventional techniques, which essentially translates to a better head start for tissue segmentation. But it should be pointed out that, despite the improved image quality, a dedicated algorithm for neonatal brain segmentation is still crucial.

Numerous brain image segmentation methods have been proposed, but they are mainly developed for adult brains [Pham et al., 2000]. For the case of neonatal brains, existing methods include clustering [Anbeek et al., 2008] and population-atlas-based segmentation approaches [Prastawa et al., 2005; Warfield et al., 2000; Weisenfeld and Warfield, 2009; Xue et al., 2007]. Affected by low image quality and also large intensity variability between nonmyelinated and myelinated WM, clustering-based methods relying solely on image intensities can be very limited in terms of segmentation performance. In light of this, atlas-based methods employ population atlases as spatial priors for segmentation guidance. Existing atlases are usually built by averaging a group of spatially normalized segmented images, which we refer to as population atlas. This approach is straightforward and easy to implement but has several inherent drawbacks. First, the atlases are in general blurry, especially in the cortical region. This is an inevitable consequence of averaging a group of images with varying anatomical structures, and hence the atlases fall short in providing sufficient prior information, especially when fine tissue structures are concerned. Second, a recent study points out that an atlas built from images with anatomy similar to the to-be-segmented image can achieve better segmentation performance than atlases built from randomly selected images [Aljabar et al., 2009]. Hence, weighting population images based on their similarity to the query image in building an atlas is a more appropriate approach than equal weighting. Third, the atlases are often aligned to the subjects utilizing affine or low degrees-of-freedom nonlinear transformation, which cannot guarantee topological correspondences and thus jeopardizes segmentation accuracy. In summary, a good atlas for guiding segmentation should have the following two properties: (1) contains a wide range of coarse-to-fine structural information to maximize guidance capacity, and (2) capable of achieving sufficient homology with respect to the subject in order to minimize guidance error. To meet these requirements, we construct a hybrid atlas, by incorporating unique subject-specific cortical information from the to-be-segmented image in addition to a population atlas, with the goal of capturing sufficient coarse and fine brain structural information in neonatal images.

To construct such a hybrid atlas, a two-phase strategy is proposed. First, the subject-specific cortical GM folding patterns are extracted. Cortical folding patterns are complex and are posed as a difficult segmentation problem considering the fact that population atlas often appears blurry and provides inadequate cortical tissue prior information. It can be observed from the acquired neonatal images (shown in Fig. 7a) that the fine structures of the cortical folding are well delineated and hence should be properly leveraged as a cortical prior. To this end, we modify a vessel-tracking method [Frangi et al., 1998] to enhance the cortical patterns, which will serve as subject-specific cortical GM characteristics. Second, a population atlas is constructed to provide global tissue spatial prior information and to mitigate bias which is prone to happen when the prior is derived from only a particular image.

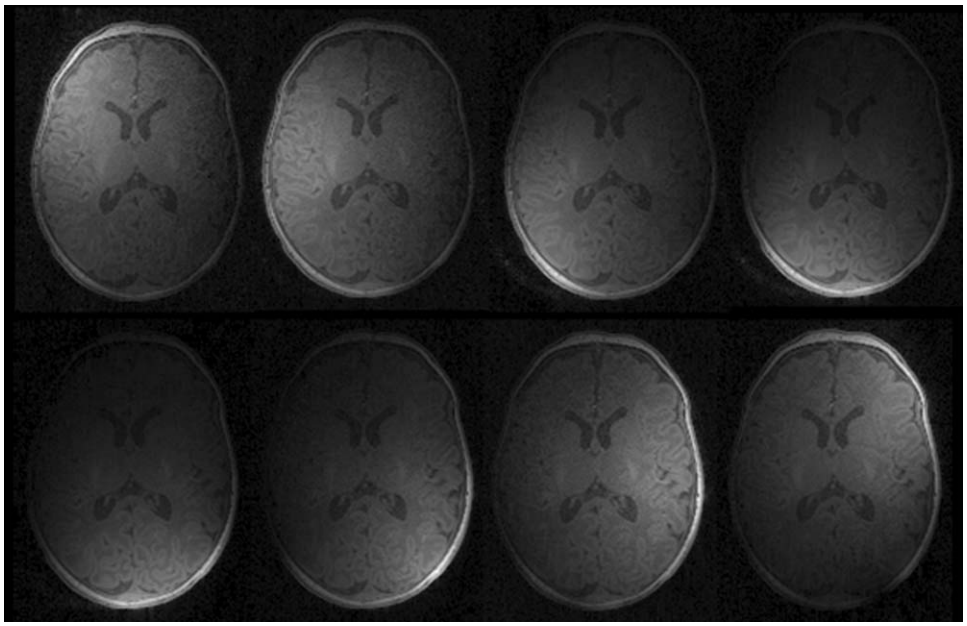

Figure 1.
T1 MR images obtained from the eight phased array coil elements. Each image shows different sensitivity region, which corresponds to the individual location of each coil.

Combining the results from these two phases, a hybrid atlas can be constructed to take advantage of both pieces of information and to provide higher guidance power for segmentation of major and minor brain structures.

The effectiveness of our framework is validated using visual inspection and also quantitative comparison with manual segmentations, as well as two population-atlas-based methods. Experimental results indicate that by enhancing image acquisition and improving atlas building, neonatal segmentation accuracy is improved. The rest of the article is organized as follows. The phased array coil imaging technique is first introduced, and then the proposed tissue segmentation scheme is detailed. Experimental results are provided, followed by the conclusion of this article.

IMAGING WITH PHASED ARRAY COIL

In MR imaging, there is a trade-off between SNR and image resolution [Mark et al., 1999]. It can be described as:

$$\mathrm{SNR/voxel} \propto \frac{\Delta x \Delta y \Delta y \sqrt{N_{\mathrm{acq}}}}{\sqrt{\frac{\mathrm{BW}_{\mathrm{read}}}{N_x N_y N_z}}} \tag{1}$$

where Δx, Δy, and Δz are the voxel sizes, N_{acq} is the number of acquisitions, $\mathrm{BW}_{\mathrm{read}}$ is the readout bandwidth dependence, and N_x, N_y, and N_z are the number of k-space samples. The equation indicates that, if one increases the image resolution (i.e., decreasing the voxel sizes Δx, Δy, and Δz), the SNR decreases accordingly. If the SNR-resolution trade-off is improved, the acquisition time needs to be increased. A parallel imaging technique is introduced later to leverage this trade-off to enhance both the SNR and image resolution without lengthening the acquisition time, which is critical especially for neonates with no sedation during the scan.

A phase array coil consisting of multiple small coils can be employed to improve SNR. A volume coil provides uniform coverage of a large ROI with the cost of a lower SNR. On the other hand, a small surface coil covers a small anatomical region with much higher signal sensitivity, leading to higher SNR compared with a volume coil. Multiple mutually decoupled surface coils are usually arranged in a way to provide a full coverage of a large ROI. Signal acquired by these coils can be combined to yield better image quality with higher SNR and within a relatively short acquisition time, as demonstrated in previous studies [Roemer et al., 1990; Wald et al., 1995]. The overall shape of the neonatal phased array coil used in this study was designed according to the average brain shape estimated from 60 normal pediatric subjects.

After acquiring a series of images by a number of coil elements (such as the eight coil elements in Fig. 1), the question of how to combine these images needs to be addressed. Because of the limited reachable volume of each surface coil, voxels close to the coil yield better SNR and better tissue contrast, compared with those farther away. Sum of square metric is widely used to directly combine these coil

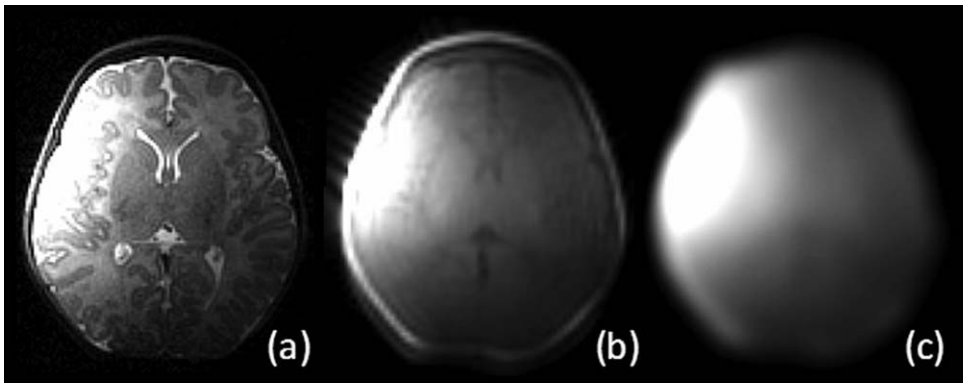

Figure 2.
Illustrations of (**a**) coil image, (**b**) coil profile image, and (**c**) estimated sensitivity map. Note that, to obtain (c), non-brain tissues are first removed to better concentrate on the brain parenchyma.

images [Roemer et al., 1990]. A better approach is by utilizing a coil profile, which can be obtained concurrently in the same scanning session by taking a low-resolution scan of the whole brain, as a reference image to generate a sensitivity map for each coil. An optimal weighting scheme can then be devised to take full advantage of each image in generating a final single combined image.

In this study, we propose a segmentation-oriented multichannel image combination strategy. This is achieved by controlling the proportion of sensitivity map used in combination, with the goal of constructing a high GM-WM contrast image for facilitating the subsequent tissue segmentation. Specifically, the phased array coil consists of 8 receiving channels (see Fig. 1). Their acquired images, denoted as C_i, $i = 1,\ldots,8$ are accompanied by their respective sensitivity profiles, denoted as P_i, $i = 1,\ldots,8$, respectively. Although the resolution of the coil profile images is low, they still contain too much structural information to be used as sensitivity maps. To estimate a sensitivity map from the respective coil profile P_i, a low-pass filter [Lin et al., 2003] is employed (Fig. 2c). For simplicity, the same notation P_i is used to also denote the generated sensitivity map for each coil. On the basis of sensitivity maps, a high-quality image I can be reconstructed from the acquired coil images:

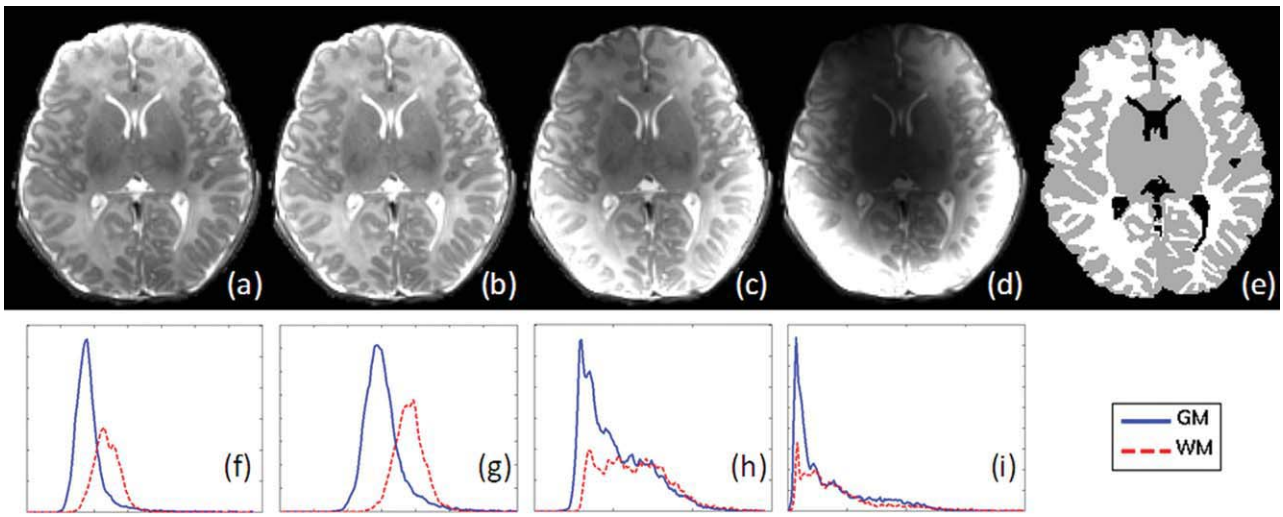

Figure 3.
Image reconstruction results with different q values. (**a**–**d**) show the results when q is set as 0, 0.3, 1, 2, respectively. (**f**–**i**) are the GM and WM intensity distributions corresponding to (a–d), obtained with the help of a manually segmented image (**e**). [Color figure can be viewed in the online issue, which is available at wileyonlinelibrary.com.]

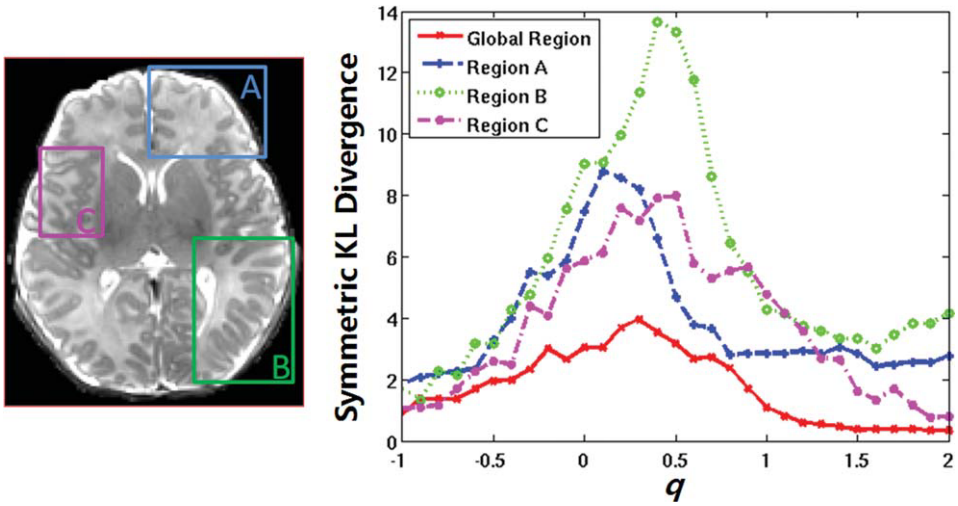

Figure 4.
Symmetric KL divergence between the GM and WM histograms for different q values in the global region, regions A, B, and C, respectively. [Color figure can be viewed in the online issue, which is available at wileyonlinelibrary.com.]

$$I = \left(\frac{1}{N}\sum_{i=1}^{N}\left(\frac{C_i}{P_i}P_i^q\right)^2\right)^{\frac{1}{2}} = \left(\frac{1}{N}\sum_{i=1}^{N}\left(C_i P_i^{q-1}\right)^2\right)^{\frac{1}{2}} \quad (2)$$

where N is the number of coils, which is 8 in this study. As we can see from this equation, the image C_i is first corrected via inverse weighting by P_i, which is effectively an intensity equalization process, and is then further weighted by the sensitivity map with exponent raised to q, i.e., P_i^q. The parameter q reflects the weight assigned to each of the sensitivity maps in the reconstruction. For example, when q is 0, the 8 intensity-corrected images are combined in a spatially uniform manner. When q is 1, we have the special case of directly combining coil images with sum-of-squares metric without the help of sensitivity maps as $I = \left(\frac{1}{N}\sum_{i=1}^{N}(C_i)^2\right)^{\frac{1}{2}}$, which is widely used in the previous studies [Roemer et al., 1990]. As q decreases (or increases), voxels farther away from the coils will be increasingly emphasized (or suppressed). Determining a suitable q value will give us a balanced image with good whole brain tissue contrast. Sample results with q = 0,0.3,1,2, are shown in Figure 3a–d. With the help of a manually segmented image, as shown in Figure 3e, the intensity distributions of GM and WM can be computed, as shown in Figure 3f–i. These distributions are indicative of how well GM and WM can be separated. Generally, the farther the GM and WM curves are, the easier the segmentation will be. We employ the symmetric Kullback–Leibler (KL) divergence to measure the difference between the GM and WM distributions. With q values ranging from -1 to 2 with a 0.1 interval, the KL divergence curve for global region is shown in Figure 4. The peaks of the KL divergence curve falls within the q interval of 0–0.5. To verify this finding, we selected some small regions such as regions A, B, and C in Figure 4, and found that their respective peaks of the parameter q are actually in the same range. We chose a moderate value in this range as $q = 0.3$ in this study. In this way, we can better combine the multichannel images than the traditional sum-of-square technique.

Quality Comparison Between Images Acquired Using Volume Coil and Phased Array Coil

To better demonstrate the image quality improvement brought forth by the phased array coil compared with images acquired from a volume coil used in our previous neonatal studies, we collect images utilizing both coils with an MPRAGE sequence using a 3T Siemens scanner. A summary of the MR imaging parameters are provided in Table I. It can be seen that, the image resolutions of both T1 and T2 are higher using the phased array coil than that of the volume coil, without significantly lengthening the acquisition time.

The image quality can also be investigated by calculating the SNR. For this purpose, the SNR is defined as averaged intensity ratio of the given regions for a certain tissue and the background [Mark et al., 1999]:

$$\mathrm{SNR} = \frac{\mu_{\mathrm{tissue}}}{1.25 \times \mu_{\mathrm{background}}} \quad (3)$$

where μ is the mean intensity of the given regions. Notice that the SNR is spatially dependent for the phased array coil and is more uniform for a volume coil. We manually delineate four different regions of interest for the GM,

TABLE I. T1 and T2 imaging parameters for volume coil and phased array coil

	T1							T2						
	TR (ms)	TE (ms)	Flip angle	Acquisition matrix	Resolution (mm^3)	Slice	Acquisition time (min)	TR (ms)	TE (ms)	Flip angle	Acquisition matrix	Resolution (mm^3)	Slice	Acquisition time (min)
Volume coil	1820	4.38	7	256 × 192	1 × 1 × 1	160 sagittal	5.51	7380	119	150	256 × 128	1.25 × 1.25 × 1.95	70 transverse	5.36
Phased array coil	1900	4.38	7	256 × 192	0.79 × 0.79 × 0.8	144 sagittal	4.53	9280	119	150	256 × 128	1 × 1 × 1.3	87 transverse	4.58

WM, and background to obtain the mean SNR values (see Fig. 5).

The resulting SNR values of 10 images taken using the phased array coil and another 10 images using volume coil (with all subjects randomly selected from a large dataset) are shown in the right of Figure 5. The SNR values are higher by using phased array coil than that of volume coil for both GM and WM. In summary, by introducing a phased array coil technique for neonatal MRI acquisition and proposing a new multichannel image combination strategy, high-resolution images can be acquired with high SNR at a sufficiently short acquisition time, which provides a good head start for the problem of neonatal brain MR segmentation.

HYBRID ATLAS CONSTRUCTION AND TISSUE SEGMENTATION

Because of low tissue contrast and large overlap of GM and WM intensity distributions in neonatal brain images, additional tissue priors need to be employed to provide helpful cues in tissue segmentation. Unlike the widely used population atlases, a hybrid atlas approach is proposed in this article. In particular, our atlas combines subject-specific cortical GM distribution with a neonatal population atlas. The neonatal tissue segmentation problem is then formulated as an iterative hybrid atlas construction and image segmentation problem. The segmentation framework consists of three major steps, shown as steps (a–c) in Figure 6. The first step involves the extraction of the cortical GM sheet in neonatal image, which will serve as a cortical GM confidence map to aid the following differentiation between GM and WM. This can be achieved via a second-order geometric structure identification approach. The second step involves the construction of the neonatal population atlas by nonlinear registration of a large group of presegmented neonatal images, weighted by their similarities to the to-be-segmented image in cortical GM region provided by the confidence map. Finally, the cortical GM prior of this subject is combined with the weighted neonatal population atlas, resulting in a hybrid atlas. The registration accuracy between the warped atlas and the to-be-segmented image is refined by a simultaneous registration and segmentation process. All details are given in the following subsections.

Before segmentation, all images are preprocessed using a standard procedure. Non-brain tissues (such as skull and dura) are stripped with brain surface extractor [Shattuck and Leahy, 2001], followed by manual editing with ITK-SNAP software [Yushkevich et al., 2006] to ensure accurate removal of non-brain tissues. The cerebellum and brain stem are also manually removed so that we can focus on the tissue segmentation of only the cerebrum [Kwon et al., 2003]. Bias correction is performed in all images with N3 method [Sled et al., 1998] to reduce the impact of intensity inhomogeneity and thus improve the performance of the subsequent tissue segmentation.

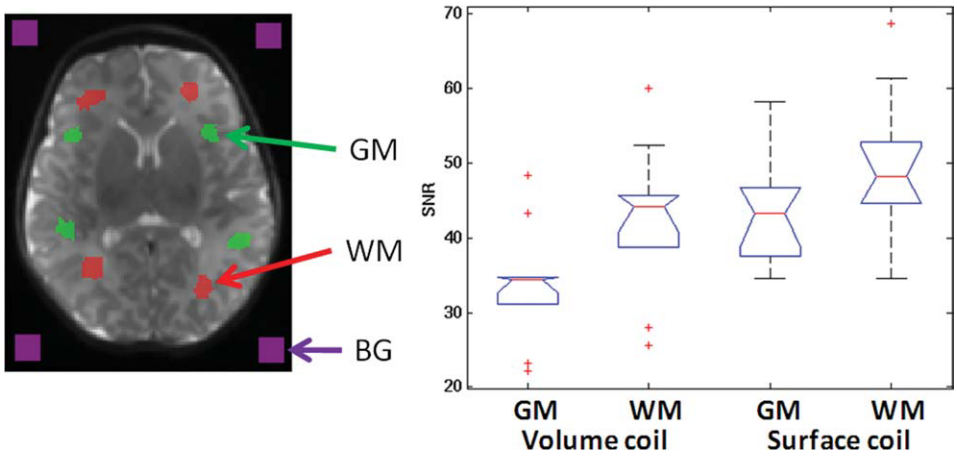

Figure 5.
Left: Regions of interest on the GM, WM, and background (BG). Right: SNR values for GM and WM of 10 images taken with the conventional volume coil, and 10 images with the surface coils. [Color figure can be viewed in the online issue, which is available at wileyonlinelibrary.com.]

Extraction of Cortical GM Confidence Map

Brain cortical convolution pattern is unique for each individual. It is hence desirable that this pattern can be enhanced to formulate a more informed segmentation algorithm especially when the cortical region is concerned. Segmentation of cortical region is often the weak spot of population-based atlases, since fine details in this region are often smoothed out by the averaging process in constructing the atlases due to large intersubject variability. Approaches based on intensities alone are quite limited in revealing the cortical pattern, since the intensity distributions of GM and WM are often overlapping and not separable. One way of revealing this pattern is by utilizing geometric measurements [Kirbas and Quek, 2004], which reflect the shape relationship of the anatomical structures and not solely the intensity differences. They can delineate fine structures with seemingly similar intensities and can hence enhance local GM/WM intensity contrast especially in the cortical region, where we can often find rapid changes of geometric patterns. The first-order intensity derivative, i.e., gradient, measures the major local direction of intensity change and can only give us information on whether or not there is a structure. The second-order derivative, as is encapsulated in the Hessian matrix, can furnish further information such as the curvature of the local structure. We thus employ the Hessian matrix for building structural filters to delineate the cortical patterns in the brain images, although other similar techniques may be also applicable. Details are given later.

First, the to-be-segmented image is combined with Gaussian smoothing to reduce the effect of noise. Specifically, for each voxel x, a Gaussian kernel σ is convolved with the original image I_0:

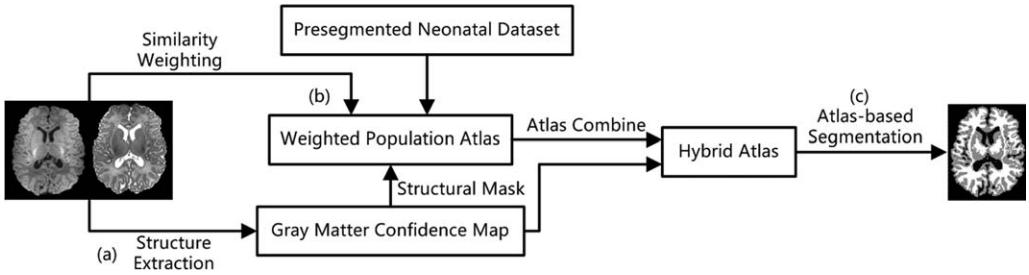

Figure 6.
Schematic diagram of the proposed neonatal segmentation framework. (**a**–**c**) shows the three major steps involved. The T1 and T2 images on the left are the inputs, and the segmented image on the right is the output.

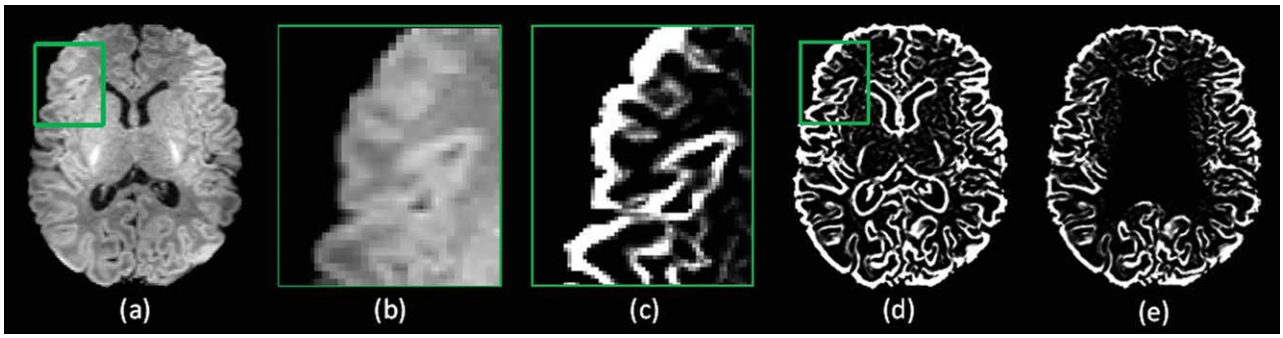

Figure 7.
Cortical GM confidence map extraction. Original T1 image (**a**), an enlarged region (**b**), GM confidence map of the enlarged region (**c**), whole GM confidence map (**d**), and final cortical GM confidence map with subcortical regions removed by the topological template shown in Figure 8. [Color figure can be viewed in the online issue, which is available at wileyonlinelibrary.com.]

$$I(x) = I_0(x) \times G(x|\sigma) \tag{4}$$

where σ is the scale-space parameter and set as 0.75 in this article. A larger σ corresponds to a coarser image.

Then, for the Gaussian smoothed image I, its local structure can be analyzed with Taylor approximation up to the second order in a neighborhood defined by scale r:

$$I(x + \Delta x) \approx I(x) + \Delta x^T \nabla(x) + \frac{1}{2}\Delta x^T H(x) \Delta x \tag{5}$$

where x is a current voxel, $x + \Delta x$ is a neighboring voxel in the range of scale r; ∇ is the gradient vector, and H the Hessian matrix. H can be decomposed in the form of:

$$H\mu_k = \lambda_k \mu_k \tag{6}$$

where μ_k and λ_k are the k-th eigenvector and eigenvalues, respectively, and k 1,2,3 in the 3D case.

The three eigenvectors can be used to form an ellipsoid, which describes the local structures. Several structures can be identified by the relative amplitudes of the eigenvalues, namely line-, plate-, and blob-like structures. If the three eigenvalues are comparable, the local structure around x is similar to a blob. Assuming $|\lambda_1| \leq |\lambda_2| \leq |\lambda_3|$, if $|\lambda_1| \ll |\lambda_2|, |\lambda_3|$, local intensities change significantly in two directions and so it is a line-like structure. If $|\lambda_1|, |\lambda_2| \ll |\lambda_3|$, the local structure is plate-like. In human brain, cortical GM covers the WM in a sheet-like fashion with a thickness ranging from 1.5 to 5 mm. By setting an appropriate scale r (e.g., 3.5 mm chosen in this article), the neighbor of given GM voxel contains other tissues like WM or CSF. In neonatal T1 images, GM has higher intensity than that of WM and CSF. The GM voxel could be identified by detecting bright structures from dark backgrounds. If this scale r is too small, the structure is blob-like and cannot be distinguished from other blob-like structures in WM and CSF. Because of this, we fine-tune this specific filter width to facilitate the following GM structure extraction. Meanwhile, because the cortical folding curvature is sharp at the tip of gyri and the valley of sulci, but flat at locations between them, both line- and plate-like local structures exist in the cortical GM sheet. Hence, we compute both structures and take the maximum as to form the GM confidence map. Note that, due to the existence of a large amount of irregular structures, the line- and plate-like structures cannot be simply extracted. We thus define two geometric ratios $\Re_B$ and $\Re_A$:

$$\Re_B = \frac{|\lambda_1|}{\sqrt{|\lambda_2 \lambda_3|}}, \Re_A = \frac{|\lambda_2|}{|\lambda_3|} \tag{7}$$

where $\Re_B$ accounts for the deviation from a blob-like structure, and $\Re_A$ distinguishes plate-like structure from line-like structure.

For extracting bright structures from a dark background, such as extracting GM from a T1 image of a neonate, in which GM has higher intensity than adjacent WM and CSF as shown in Figure 7, λ_2 and λ_3 should be negative for line structure, and λ_3 should be negative for plate structure. On the contrary, for extracting dark structure from a bright background, such as extracting GM from a T2 image, these

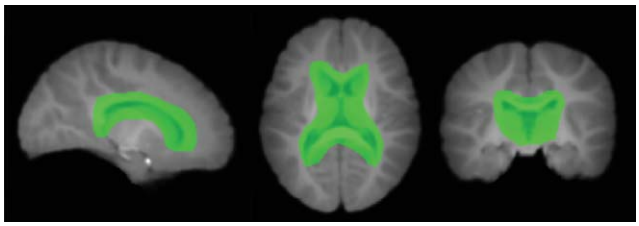

Figure 8.
Topological template, used as a subcortical mask, displayed in three orthogonal sections. [Color figure can be viewed in the online issue, which is available at wileyonlinelibrary.com.]

eigenvalues should be positive. The line and plate filters for extracting bright structures are given by:

$$V_{\text{line}} = \left(1 - \exp\left(-\frac{\Re_A^2}{2\alpha^2}\right)\right)\exp\left(-\frac{\Re_B^2}{2\beta^2}\right)\left(1 - \exp\left(-\frac{S^2}{2c^2}\right)\right), \quad \text{if} \quad \lambda_2 < 0 \text{ and } \lambda_3 < 0; \text{ otherwise } V_{\text{line}} = 0 \quad (8)$$

$$V_{\text{plate}} = \exp\left(-\frac{\Re_A^2}{2\alpha^2}\right)\exp\left(-\frac{\Re_B^2}{2\beta^2}\right)\left(1 - \exp\left(-\frac{S^2}{2c^2}\right)\right), \quad \text{if } \lambda_3 < 0; \text{ otherwise } V_{\text{plate}} = 0 \quad (9)$$

$$S = \sqrt{\sum_{j \le D} \lambda_j^2} \quad (10)$$

where D is the dimension of the image (in our case $D = 3$), and S is the second-order structureness measurement defined to constrain the magnitudes of the derivatives. α, β, and c are the parameters which control the structure sensitivity of the filters. In this article, α, β are fixed at 0.5, and c is set as half the value of the maximum Hessian norm. The aforementioned equations are applied to each voxel and the probability maps returned by them indicate the degrees of structureness of each voxel. It is worth noting that by using only the plate filter, there will be some discontinuities in the cortical GM structure probability map. Hence, we employ both the line and plate filters, and determine the structure at each voxel based on the maximal value between the two values given by the two filters.

The detected GM profile is shown in Figure 7. Part of the profile is enlarged, as shown in Figure 7b,c, for better demonstrating the patterns. Notice that, for the GM profile in Figure 7d, it includes not only the cortical GM convolution pattern, but also the boundary of the ventricle. This is because the adjacent brain tissues are brighter than the ventricular region, and so the boundary of the ventricle is also detected. For our case, this portion of the GM profile is not desirable because it may result in a wrong subcortical GM prior. To remove it, a topological template is employed. This template is obtained by manually delineating the subcortical region, ventricle inclusive, on a structural atlas built by averaging a group of normalized T1 images. Then this topological template is registered to the neonatal image to mask out the subcortical region in the detected GM profile map (see Fig. 8). In this way, we retain only the cortical GM (Fig. 7e) for providing additional subject-specific cortical GM spatial information for segmentation. Notice that the subcortical region may not be masked out perfectly due to possible registration error, but this imperfectness has only minor influence on the subsequent segmentation results because the tissue distribution will be estimated in a way, which is insensitive to local variation.

Construction of Similarity-Weighted Neonatal Population Atlas

Because of the rapid development of neonatal brains especially during the first year of life, adult atlases, or even those constructed from pediatric brains, are not directly applicable for segmentation of neonatal brain images due to large anatomical differences. For constructing a population atlas, we use a dataset of T2 MR images of 68 neonatal subjects (38 male and 30 female), along with their segmentation results and also GM, WM, and CSF tissue probability maps from our previous study [Shi et al., 2010]. Note that these images are used only for generating the neonatal population atlas.

Image normalization for population

Numerous approaches for atlas construction have been proposed [Altaye et al., 2008; Joshi et al., 2004]. Some earlier approaches involve the registration of all images onto a template (usually chosen from one of the subjects) and then averaging the aligned images [Warfield et al., 2002]. Approaches as such are bias prone, since the chosen template often has dominance over the final atlas. A better alternative is to introduce the groupwise registration strategy, to construct a data-driven representative atlas.

To groupwisely normalize all subjects onto a same coordinate space, two steps are performed. Affine transform is first used for rough alignment. Then, a nonlinear registration is performed to more effectively remove the intersubject variability. To avoid bias in registration due to the preselection of template, we adopt a groupwise registration approach, similar to [Joshi et al., 2004], to transform all subjects to their group center, to which all subjects can be warped with the minimum overall transformations. Note that we used T2 MR images for spatial normalization.

Specifically, we first average the affine transformed images I_i, $i = 1,\ldots,N$, to obtain an initial template T^0. Then a nonlinear registration algorithm, called HAMMER [Shen and Davatzikos, 2002], is performed to register each subject to the current template T^{t-1}, resulting in the warped subjects T_i^t and taking their averaged image as an updated template T^t. By iteratively alternating between subject alignment and template generation, all images will be eventually warped onto a common space after convergence of registration.

Similarity weighting

The traditional way of generating an atlas from the normalized images of a population is by equally averaging the subject images. In such approach, structures with low intersubject anatomical variances will be retained (like the thick WM branches), and regions with high anatomical variances will be blurred (such as the cortical GM convolutions). It was recently shown that atlases built by images with similar anatomy have better guidance power for segmentation

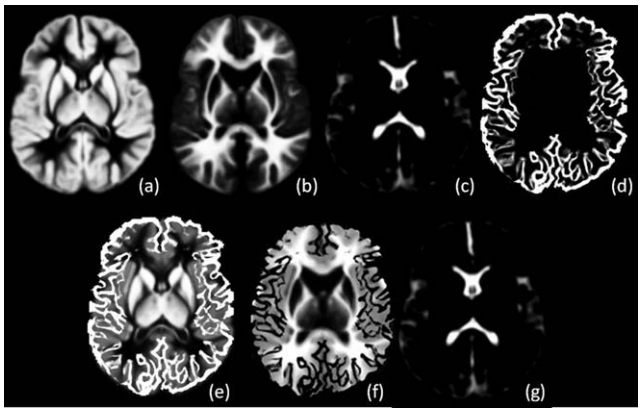

Figure 9.
Illustration of population atlas, cortical GM confidence map, and their hybrid atlas. (**a**–**c**) GM, WM, and CSF probability maps of population atlas, (**d**) cortical GM confidence map constructed from the to-be-segmented MR image, and (**e**–**g**) resulting GM, WM, and CSF probability maps of hybrid atlas.

[Aljabar et al., 2009]. Motivated by this, we utilize image similarity values between the population images and the to-be-segmented image as weighting factors to build a neonatal population atlas which is more similar to the new subject, for taking full advantage of the population data. Moreover, to make the cortex provide relatively more specific structural information in atlas building, we first binarize the GM confidence map (obtained from the previous section) by choosing voxels with at least 90% confidence level, and then use it as an image mask to measure the image similarity only in the cortical GM regions. This allows us to generate a subject-specific atlas with emphasis on cortical regions, thus leading to better segmentation with a subsequent atlas-based segmentation algorithm. Specifically, for similarity comparison, the to-be-segmented image is warped to the template generated in the last section by first performing affine transform and then utilizing an intensity-based nonrigid registration [Shen, 2007].

Many metrics are available for image similarity measurements, such as cross correlation, mutual information, and mean square differences. We choose the popular mutual information as similarity measure in this article:

$$w_i = \frac{H(Q^t, I_i^t)}{\sum_i H(Q^t, I_i^t)} \tag{11}$$

$$P^k = \frac{\sum_i w_i I_i^t(k)}{\sum_i w_i}, k \in \{\mathrm{WM}, \mathrm{GM}, \mathrm{CSF}\} \tag{12}$$

where I_i^t is the i-th aligned image (after t-th iteration); w_i is the weight for i-th image; $H(\cdot)$ is the mutual information function; Q^t is the to-be-segmented query image on the template space; and P^k is the resulting weighted average probability map for GM, WM, and CSF, respectively. After the aforementioned similarity weighting procedure, the resulting subject-specific atlases are shown in Figure 9a–c.

Joint Registration and Segmentation

The neonatal atlas is modified according to the GM confidence map. For a given voxel x in the neonatal atlas, there are three tissue probabilities P_x^{GM}, P_x^{WM}, and P_x^{CSF} ($P_x^{\mathrm{GM}} + P_x^{\mathrm{WM}} + P_x^{\mathrm{CSF}} \quad 1$). Note that voxels in the cortical region that show high confidence as GM (as judged by the cortical GM confidence map C_x^{GM}) should have their GM probabilities increased, and those with low confidence should have their GM probabilities reduced. Their CSF probabilities should be kept unchanged and WM probabilities adjusted accordingly. In the subcortical region as labeled by the topological mask, these probabilities are kept unchanged. For cortical regions (where the topological mask is 0), we combine the hybrid atlas as follows:

$$P_{x,\mathrm{hybrid}}^{\mathrm{GM}} = \left(P_x^{\mathrm{GM}} + C_x^{\mathrm{GM}}\right)/2 \tag{13}$$

$$P_{x,\mathrm{hybrid}}^{\mathrm{CSF}} = P_x^{\mathrm{CSF}} \tag{14}$$

$$P_{x,\mathrm{hybrid}}^{\mathrm{WM}} = 1 - P_{x,\mathrm{hybrid}}^{\mathrm{GM}} - P_{x,\mathrm{hybrid}}^{\mathrm{CSF}} \tag{15}$$

where the final GM probability map $P_{x,\mathrm{hybrid}}^{\mathrm{GM}}$ is combined with the WM and CSF probability maps to form a hybrid atlas as shown in Figure 9e–g.

After obtaining the hybrid atlas, an atlas-based segmentation algorithm [Ashburner and Friston, 2005] is applied to perform tissue segmentation on the neonatal subjects. In brief, the algorithm involves alternating among bias correction, tissue classification, and atlas-to-subject registration. In particular, a mixture of Gaussians is used to model the distribution of each brain tissue. The hybrid atlas represents the prior probabilities of existence of different tissues at each image location. Bayes rule is used to combine these priors with tissue probabilities derived from voxel intensities to provide the posterior probability, thus giving the tissue membership probabilities for each voxel. Based on the segmentation results, the registration between the atlas and the neonatal subject can be refined by another round of deformable registration [Shen and Davatzikos, 2002], to further reduce registration error and thus bring the atlas closer to the neonatal subject for more accurate segmentation guidance, as is done in most joint registration and segmentation algorithms [Yezzi et al., 2003]. Bias correction, tissue segmentation, and atlas- to-subject registration are iterated until convergence.

EXPERIMENTAL RESULTS

A total of 10 neonates with manual segmentation results are used for performance evaluation of the proposed neonatal brain segmentation framework. They consist of five

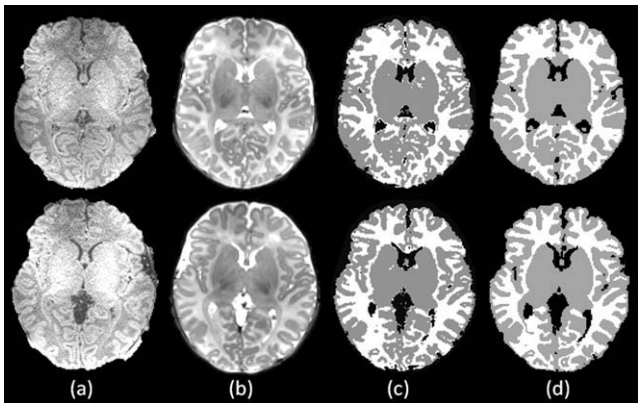

Figure 10.
Illustration of (**a**) T1 image, (**b**) T2 image, and segmentation results yielded by (**c**) the proposed segmentation method and (**d**) a manual rater.

males and five females with postnatal age range of 0.5–1.9 months. T1 and T2 images were acquired by using a 3T head-only MR scanner with scanning parameters provided in Table I. In addition, a low-resolution spin density weighted 3D FLASH sequence was employed to obtain eight coil sensitivity profiles. The constructed T1 and T2 neonatal brain images are shown in Figure 10a,b. T2 image is chosen for both automatic and manual segmentation, because it has better tissue contrast than T1 image in neonatal stage as also demonstrated in our previous study [Shi et al., 2010]. Manual segmentations were performed on typical brain slides, including two sagittal slices, three coronal slices, and three axial slices, selected by a trained rater. All these selected sliced images were first segmented by an intensity clustering method, and then manually edited with the ITK-SNAP software [Yushkevich et al., 2006]. The typical manual segmentation results could be observed in Figures 10d, 12e, 14a, and 16e.

Visual Inspection

Representative segmentation results yielded by the proposed method and a manual rater on two subjects are shown in Figure 10. Also shown are their original T1 and T2 images for comparison. The fine structures in neonatal image, especially in the T2 image, are well preserved after segmentation and are comparable with those of manual segmentations. Accurate tissue segmentation facilitates further cortical surface reconstruction (see Fig. 11).

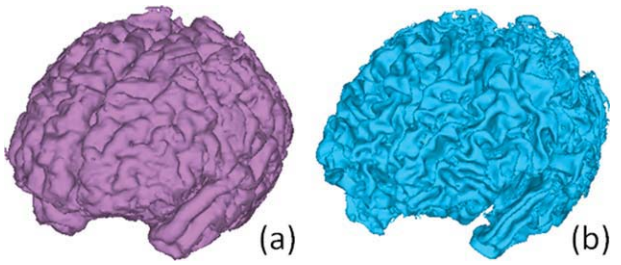

Figure 11.
Surface rendering of tissue segmentation result of one subject. (**a**) Gray matter surface and (b) white matter surface. [Color figure can be viewed in the online issue, which is available at wileyonlinelibrary.com.]

Quantitative Comparison with Manual Segmentations

To quantitatively evaluate the performance of our proposed segmentation method, manual segmentation was performed on all 10 neonates, and the obtained results are used as the ground truth for evaluating the automatic segmentations. For quantitative comparison, the Dice ratio (DR) [Dice, 1945], $DR = 2|A \cap B|/(|A| + |B|)$, is employed to measure the overlap rate between the manual segmentation A and automatic segmentation B. The DR ranges from 0 to 1, corresponding to the worst and the best segmentation results. The DRs of the proposed method for GM, WM, and CSF are shown in Figure 13, as 0.89 ± 0.02, 0.89 ± 0.01, and 0.87 ± 0.03, respectively.

Quantitative Comparison with Two Population Atlases

To further evaluate the performance of our constructed hybrid atlas, two population atlases are included for comparison. In the first method (which we refer to as "Method

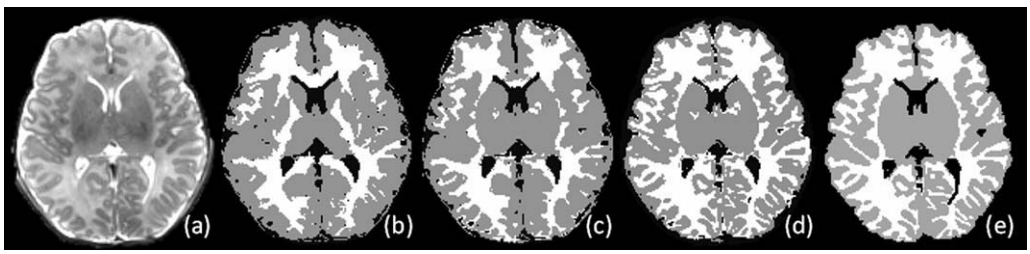

Figure 12.
(**a**) Original T2 image, and segmentation results of (**b**) Method A, (**c**) Method B, (d) our proposed method, and (e) a manual rater.

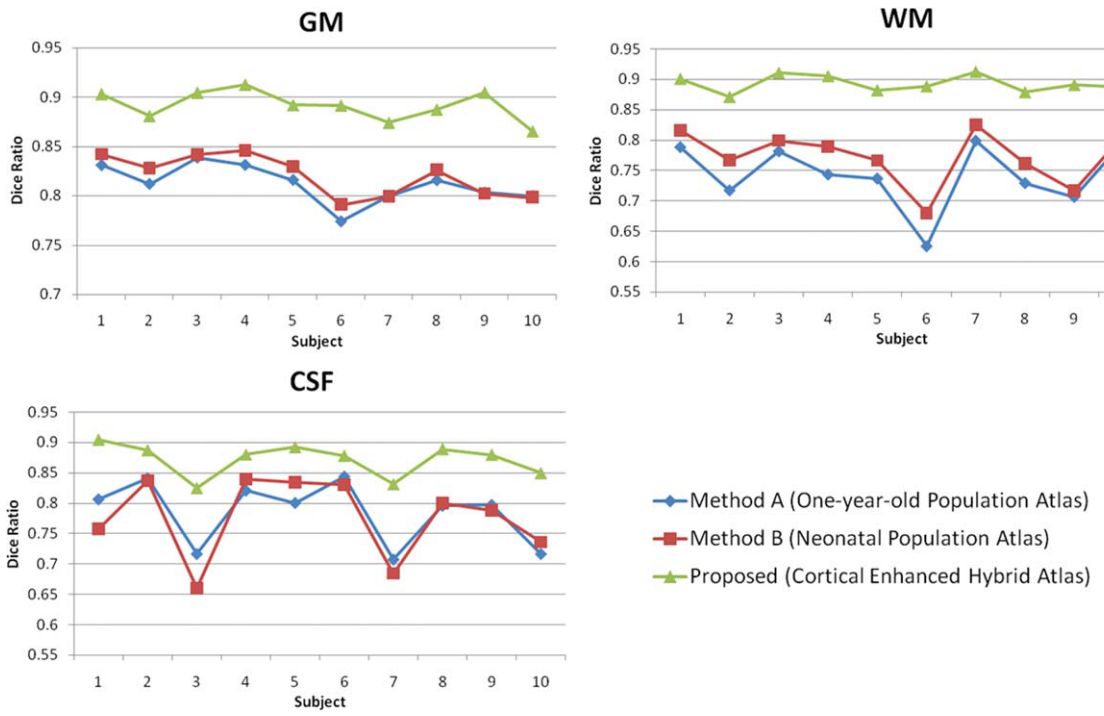

Figure 13.

Dice ratio curves by comparing manual segmentations with automatic segmentations obtained by Method A, Method B, and our proposed method, respectively. Segmentation is performed on the neonatal images acquired using a phased array coil. [Color figure can be viewed in the online issue, which is available at wileyonlinelibrary.com.]

A" later), a population atlas obtained from 76 infants ranging in age from 9 to 15 months [Altaye et al., 2008] is used to directly guide the tissue segmentation of neonatal brains. In the second method (which we refer to as "Method B" later), the neonatal atlas generated in previous section (Fig. 9a–c) is used to directly guide the brain tissue segmentation of neonates. An example of the prior probability maps used in Method B and proposed method are shown in Figure 9. It can be observed that the prior probability maps used in Method A is more blurry than that of Method B. These three methods are essentially using different atlases but with the same joint registration-segmentation algorithm for fair comparison. Figure 12 shows the corresponding segmentation results of these three methods on the neonatal brain image given in Figure 12a. It can be observed that the segmentation results obtained by our proposed method provide more detailed segmentations in both coarse and fine structures, compared with those produced by Method A and Method B.

The DR is employed to measure the overlap rate between the manually segmented images and those produced by Method A, Method B, and proposed method, respectively. The DRs of the three methods for GM, WM, and CSF are shown in Figure 13. In GM, the DR is 0.81 ± 0.02 for Method A and 0.82 ± 0.02 for Method B. In WM, the DR is 0.74 ± 0.05 for Method A and 0.77 ± 0.05 for Method B. In CSF, the DR is 0.78 ± 0.05 for Method A and 0.78 ± 0.07 for Method B. As we can observe from Figure 13, the proposed hybrid atlas-based segmentation method produces results which agree best with manual segmentation results for both GM and WM.

Besides comparing global volumes of segmented GM and WM as described earlier, the segmentation performance is further evaluated more closely in the cortical WM

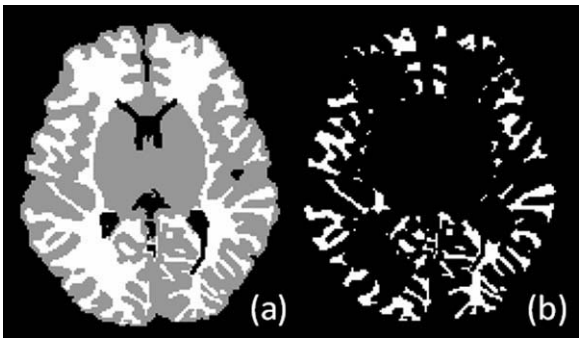

Figure 14.

Illustration of cortical WM used for evaluating segmentation, which is obtained by removing the large WM bundles. Segmentation of this part of the WM is the weakest spot of most algorithms.

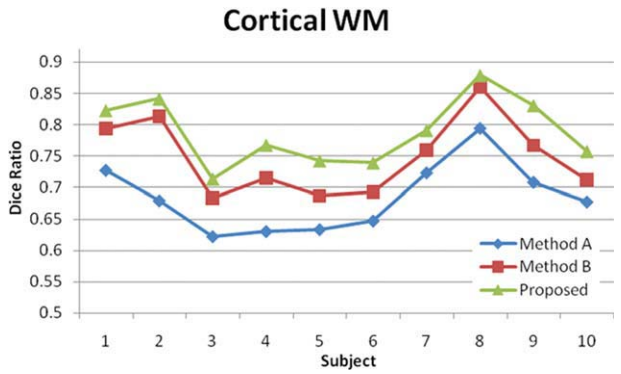

Figure 15.

Dice ratio curves by comparing manual segmentations with automatic segmentations obtained by Method A, Method B, and our proposed method, respectively. Segmentation is performed on the cortical WM region of the neonatal images acquired using a phased array coil. [Color figure can be viewed in the online issue, which is available at wileyonlinelibrary.com.]

by removing the large WM bundles, with an example shown in Figure 14. The DRs are computed for each of the three methods, and results are given in Figure 15. Again, the proposed method gives the best agreement with the manually segmented images, compared with the two population-atlas-based segmentation methods. Both visual inspection and quantitative evaluation results confirm the advantages of using the proposed hybrid atlas for neonatal brain image segmentation.

Evaluation in Neonatal Images Acquired by Conventional Volume Coil

To evaluate the performance of the proposed segmentation framework with respect to the types of coils used, 10 neonatal images acquired with conventional volume coil are used (four females and six males with postnatal age range of 0.7–1.7 months). MR scanning parameters are also provided in Table I. Compared with images acquired using the phased array coil, image quality is reduced, and cortical convolution is not clearly delineated. Representative segmentation results for one subject are shown in Figure 16, with Figure 17 showing the quantitative segmentation accuracy for each of the 10 subjects. In GM, the DR is 0.87 $\pm$ 0.02 for proposed method, 0.82 $\pm$ 0.03 for Method A, and 0.85 $\pm$ 0.03 for Method B. In WM, the DR is 0.84 $\pm$ 0.03 for the proposed method, 0.75 $\pm$ 0.05 for Method A, and 0.79 $\pm$ 0.04 for Method B. In CSF, the DR is 0.81 $\pm$ 0.04 for the proposed method, 0.76 $\pm$ 0.05 for Method A, and 0.77 $\pm$ 0.04 for Method B. As we can see, the segmentation accuracy of the proposed method on images obtained using the volume coil is better than that of Method A and Method B, although not as good as on those acquired with the phased array coil. For Method A and Method B, they showed slightly higher segmentation accuracy for images acquired with conventional volume coil. One of the reasons might be that the atlases used by their methods were constructed by images also acquired using a conventional volume coil, thus they are better suited for segmenting images obtained with similar coils.

DISCUSSION

Tissue segmentation of neonatal brain images has been a daunting task owing to poor spatial resolution resulting from small brain size, and low SNR resulting from the ongoing processes of myelination and maturation. We have shown that by introducing a phased array coil dedicated for neonatal brains, the quality of images acquired can be significantly improved by combining a set of coil images. The coils, operating in a parallel fashion, make acquisition with a sufficiently low time cost possible. This is especially crucial for the acquisition of neonatal brain images. We propose to use the KL divergence between GM and WM for estimating the optimal range of image combination parameter q. The best performance is found when q falls in the range of 0–0.5, giving the image with best contrast by combining the images from the individual coils.

Note that while the parallel imaging technique adopted in this article can help obtain high resolution and high SNR images with a short acquisition time, the fundamental difficulty of segmenting neonatal images, which are different from adult subjects due to tissue development,

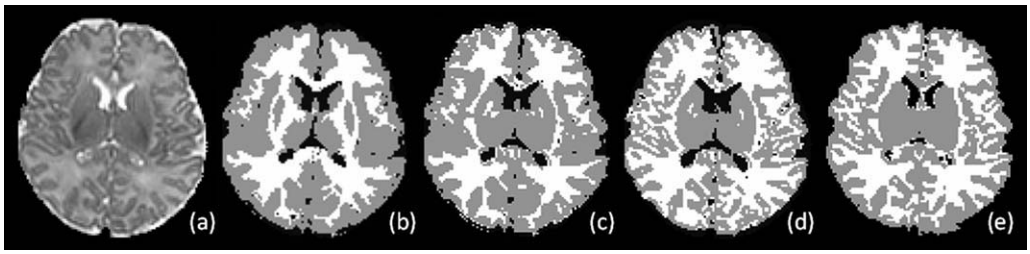

Figure 16.

(**a**) Original T2 image, and segmentation results of (**b**) Method A, (**c**) Method B, (**d**) our proposed method, and (**e**) a manual rater, for neonatal images acquired with a conventional volume coil.

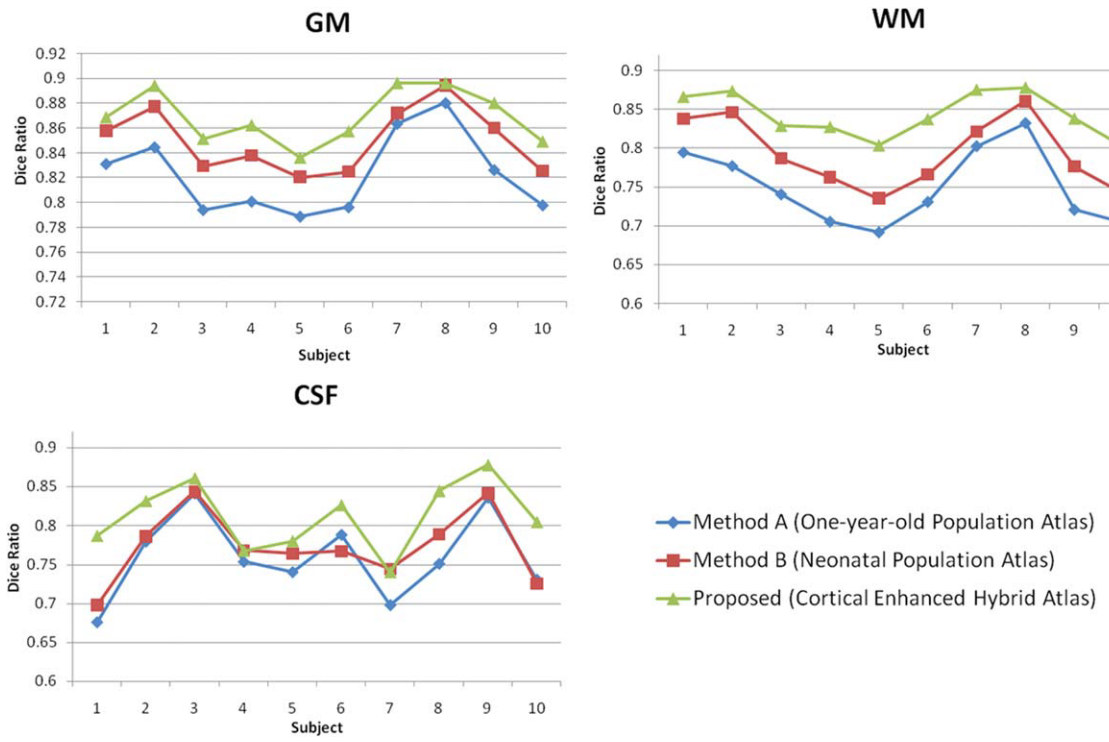

Figure 17.

Dice ratio curves by comparing manual segmentations with automatic segmentations obtained by Method A, Method B, and our proposed method, respectively. Segmentation is performed on the neonatal images acquired using a conventional volume coil. [Color figure can be viewed in the online issue, which is available at wileyonlinelibrary.com.]

remains unsolved. We developed a novel hybrid atlas-based tissue segmentation framework to remedy this problem. This hybrid atlas combines the benefits of the subject-specific cortical GM folding pattern and the neonatal population atlas. The results, compared with two population-atlas-based segmentation methods, demonstrate that the proposed approach is capable of achieving higher accuracy on images acquired with both phased array coils and conventional volume coils, especially in the cortical regions. The proposed framework is flexible and can also be applied to adult images.

In summary, we have proposed a novel way of building an atlas for tissue segmentation. Many existing atlases were constructed either by equally weighting all images or by selecting a particular image in a population. We demonstrate a way to fuse the population atlas with the subject-specific characteristics, i.e., cortical GM convolution pattern. The effectiveness of our method is confirmed by the distinction of the GM from other tissues in the cortical region, where segmentation is known to be difficult especially with population atlas-based method. The segmentation outcome using the proposed method agrees very well with that obtained from the manual rater. Using the proposed method, segmentation of a brain MR image can be performed automatically within 20 minutes. The capability of yielding relatively accurate segmentation results allows subsequent operations, such as cortical surface construction and cortical thickness measurement, to be performed more precisely.

REFERENCES

Aljabar P, Heckemann RA, Hammers A, Hajnal JV, Rueckert D (2009): Multi-atlas based segmentation of brain images: Atlas selection and its effect on accuracy. Neuroimage 46:726–738.

Altaye M, Holland SK, Wilke M, Gaser C (2008): Infant brain probability templates for MRI segmentation and normalization. Neuroimage 43:721–730.

Anbeek P, Vincken KL, Groenendaal F, Koeman A, van Osch MJ, van der Grond J (2008): Probabilistic brain tissue segmentation in neonatal magnetic resonance imaging. Pediatr Res 63:158–163.

Ashburner J, Friston KJ (2005): Unified segmentation. Neuroimage 26:839–851.

Connors SL, Levitt P, Matthews SG, Slotkin TA, Johnston MV, Kinney HC, Johnson WG, Dailey RM, Zimmerman AW (2008): Fetal mechanisms in neurodevelopmental disorders. Pediatr Neurol 38:163–176.

Dice LR (1945): Measures of the amount of ecologic association between species. Ecology 26:297–302.

Frangi AF, Niessen WJ, Vincken KL, Viergever MA (1998): Multiscale Vessel Enhancement Filtering. In: Proceedings of Medical Image Computing and Computer-Assisted Interventation (MICCAI), Springer, Berlin. LNCS 1496, pp 130–137.

Joshi S, Davis B, Jomier M, Gerig G (2004): Unbiased diffeomorphic atlas construction for computational anatomy. Neuroimage 23:151–160.

Kirbas C, Quek F (2004): A review of vessel extraction techniques and algorithms. ACM Comput Survey 36:81–121.

Knickmeyer RC, Gouttard S, Kang C, Evans D, Wilber K, Smith JK, Hamer RM, Lin W, Gerig G, Gilmore JH (2008): A structural MRI study of human brain development from birth to 2 years. J Neurosci 28:12176–12182.

Kwon MJ, Han YJ, Shin IH, Park HW (2003): Hierarchical fuzzy segmentation of brain MR images. Int J Imaging Syst Technol 13:115–125.

Lin FH, Chen YJ, Belliveau JW, Wald LL (2003): A wavelet-based approximation of surface coil sensitivity profiles for correction of image intensity inhomogeneity and parallel imaging reconstruction. Hum Brain Mapp 19:96–111.

Mark E, Haacke MRT, Brown RW (1999): Magnetic Resonance Imaging: Physical Principles and Sequence Design: Wiley-Liss.

Pham DL, Xu C, Prince JL (2000): A survey of current methods in medical image segmentation. Annu Rev Biomed Eng 2:315–337.

Prastawa M, Gilmore JH, Lin W, Gerig G (2005): Automatic segmentation of MR images of the developing newborn brain. Med Image Anal 9:457–466.

Roemer PB, Edelstein WA, Hayes CE, Souza SP, Mueller OM (1990): The NMR phased array. Magn Reson Med 16:192–225.

Shattuck DW, Leahy RM (2001): Automated graph-based analysis and correction of cortical volume topology. IEEE Trans Med Imag 20:1167–1177.

Shen D (2007): Image registration by local histogram matching. Pattern Recognit 40:1161–1172.

Shen D, Davatzikos C (2002): HAMMER: Hierarchical attribute matching mechanism for elastic registration. IEEE Trans Med Imag 21:1421–1439.

Shi F, Fan Y, Tang S, Gilmore JH, Lin W, Shen D (2010): Neonatal brain image segmentation in longitudinal MRI studies. Neuroimage 49:391–400.

Sled JG, Zijdenbos AP, Evans AC (1998): A nonparametric method for automatic correction of intensity nonuniformity in MRI data. IEEE Trans Med Imag 17:87–97.

Wald LL, Carvajal L, Moyher SE, Nelson SJ, Grant PE, Barkovich AJ, Vigneron DB (1995): Phased array detectors and an automated intensity-correction algorithm for high-resolution MR imaging of the human brain. Magn Reson Med 34:433–439.

Warfield SK, Kaus M, Jolesz FA, Kikinis R (2000): Adaptive, template moderated, spatially varying statistical classification. Med Image Anal 4:43–55.

Warfield SK, Zou KH, Wells WM (2002): Validation of image segmentation and expert quality with an expectation-maximization algorithm. In: Proceedings of Medical Image Computing and Computer-Assisted Intervention (MICCAI), Springer, Berlin. LNCS 2488, pp 298–306.

Weisenfeld NI, Warfield SK (2009): Automatic segmentation of newborn brain MRI. Neuroimage 47:564–572.

Xue H, Srinivasan L, Jiang S, Rutherford M, Edwards AD, Rueckert D, Hajnal JV (2007): Automatic segmentation and reconstruction of the cortex from neonatal MRI. Neuroimage 38:461–477.

Yezzi A, Zollei L, Kapur T (2003): A variational framework for integrating segmentation and registration through active contours. Med Image Anal 7:171–185.

Yushkevich PA, Piven J, Hazlett HC, Smith RG, Ho S, Gee JC, Gerig G (2006): User-guided 3D active contour segmentation of anatomical structures: Significantly improved efficiency and reliability. Neuroimage 31:1116–1128.